CrossMark

Twinning-Induced Elasticity in NiTi Shape Memory Alloys

Thorsten Birk[1] · Somjeet Biswas[1,2] · Jan Frenzel[1] · Gunther Eggeler[1]

Abstract Pseudoelasticity (PE) in shape memory alloys relies on the formation of stress-induced martensite during loading and on the reverse transformation during unloading. PE yields reversible strains of up to 8 % and is applied in applications such as medical implants, flexible eye glass frames, damping elements, and others. Unfortunately, PE shows a strong temperature dependence and thus can only be exploited within a relatively narrow temperature window. The present work focuses on a related process, which we refer to as twinning-induced elasticity (TIE). It involves the growth and shrinkage of martensite variants which are stabilized by dislocations, which are introduced by appropriate cold work. TIE yields reversible strains of the order of 3 %. The TIE effect does not suffer from the strong temperature dependence of PE. The weak temperature dependence of mechanical TIE properties makes TIE attractive for applications where temperature fluctuations are large. In the present work, we study the TIE effect focusing on $Ni_{50}Ti_{50}$ shape memory alloy wires. The degree of plastic pre-deformation of the initial material represents a key parameter of the ingot metallurgy processing route. It governs the exploitable recoverable strain, the apparent Young's modulus, and the widths of the mechanical hysteresis. Dynamic mechanical analysis is used to study the effects of pre-deformation on elementary microstructural processes which govern TIE.

Introduction

NiTi shape memory alloys (SMAs) show fascinating functional and structural properties [1–5]. They exhibit a high strength [6, 7] and SM effects can be exploited many times before functional and structural fatigue limit service life [8–11]. NiTi SMAs also show good corrosion resistance and biocompatibility [12, 13], such that they are attractive for medical applications. Depending on Ni-content and microstructure, they exhibit thermal (one way effect, 1WE; two way effect, 2WE) or a mechanical memory (pseudoelasticity, PE) [1–5, 14, 15]. Both types of shape memory effects rely on the martensitic phase transformation from the high temperature phase austenite (B2) to the low temperature phase martensite (B19′) during cooling/mechanical loading and on the reverse transformation during heating/unloading [1–5]. The 1WE and PE are associated with reversible deformations between 5 and 8 % [4, 5, 16].

In the present work we consider SMAs with mechanical memory. Today, more than 90 % of all commercial NiTi products exploit PE [17]. PE is applied in medical implants and instruments, flexible eye glass frames, orthodontic arch wires, and various engineering applications [18–20]. Figure 1 shows the mechanical behavior of pseudoelastic NiTi SMAs. Figure 1a shows three loading/unloading curves of a PE NiTi wire, which were obtained at different temperatures. The formation of stress-induced martensite in PE NiTi generally requires a critical stress level, and it is associated with the evolution of a stress/strain plateau.

✉ Thorsten Birk
thorsten.birk@rub.de

1 Institut für Werkstoffe, Ruhr-Universität Bochum, Bochum 44801, Germany

2 Metallurgical and Materials Engineering, Indian Institute of Technology Kharagpur, Kharagpur, West Bengal 721302, India

Springer

Fig. 1 Mechanical behavior and temperature dependence of different types of mechanical memory in NiTi SMAs. **a** Pseudoelasticity. **b** Twinning-induced elasticity (TIE)
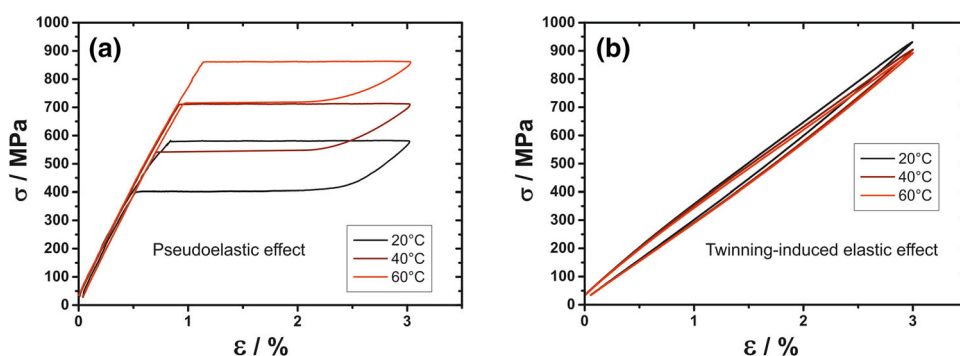
During unloading, the imposed strain is almost fully recovered as the martensite transforms back to austenite. The reverse transformation which is also associated with a stress/strain plateau occurs at lower stress levels. The loading and unloading stress strain paths in Fig. 1a limit an area, which represents a dissipated energy referred to as stress/strain hysteresis. Recently, it was shown that the width of the mechanical hysteresis in PE SMAs is governed by the crystallographic compatibility between martensite and austenite [21]. It is important to highlight that the mechanical properties of PE NiTi show a very strong Clausius–Clapeyron type of temperature dependence [22]. An increase in temperature by 10 K, for example, is associated with an increase in both plateau stresses by about 65 MPa. This trend can also be observed for the tensile curves shown in Fig. 1a. Olbricht et al. [22] showed that higher plateau stresses (caused by higher temperatures) can promote irreversible deformation based on dislocation plasticity. Therefore, PE can only be applied within a certain temperature window. Olbricht et al. [22] studied the mechanical behavior of commercial PE NiTi wires. It was observed that a good shape recovery was only obtained between 20 and 70 °C. It is clear that the strong dependence of the PE effect on temperature is problematic where applications demand large temperature windows.

Hornbogen [23] discussed the term pseudoelasticity. He pointed out that there is a type of mechanical memory in SMAs which is less well appreciated than conventional PE. It relies on the reversible growth and shrinkage of martensite twin variants in plastically deformed martensite. This effect does not involve phase transformations. Instead it exploits the stabilization of martensite twins by dislocations and the mobility of twin boundaries. During mechanical loading, preferentially oriented martensite twin variants grow on the expense of others. The external stress overcomes the stress fields of the stabilizing dislocation substructure. However, during unloading, the dislocations stress fields take over again and help to restore the original martensite twin microstructure. We refer to the associated shape recovery as twinning-induced elasticity (TIE). In the literature, TIE was referred to as "linear superelasticity" [24–26] or "twinning pseudoelasticity" [23]. Figure 1b shows examples of stress/strain curves from a NiTi SMA in the TIE state. Three experiments were performed at 20, 40, and 60 °C, Fig. 1a. One can clearly see that unlike in the case of PE, TIE is nearly unaffected by these temperature changes. Figure 1b also shows that TIE wires exhibit an almost linear stress/strain behavior, the pronounced stress plateau of the PE effect shown in Fig. 1a is not observed. However, TIE is known to provide lower reversible strains as compared to PE SMAs [23, 24, 27, 28]. Typically, strains of the order of 3 % can be fully recovered. The TIE effect is assumed to require a dislocation density in the material, which is high enough to stabilize martensite twin variants without suppressing twin boundary mobility [23]. This dislocation density can be introduced by different thermomechanical treatments like rolling, swaging, and wire drawing.

In PE SMAs, austenite grain boundaries, dislocations, and Ni-rich precipitates affect the quality of the shape memory effect [6, 8, 29–32]. During the production of commercial PE NiTi, it is of utmost importance to establish a nano-crystalline microstructure. The nanograin boundaries act as obstacles for irreversible dislocation plasticity while they do not suppress the martensitic transformation [30]. In contrast, TIE requires a strongly plastically deformed martensite [23] and the elementary processes which govern TIE occur in complex microstructures [33]. There is a good understanding of the effect of cold work on the microstructure of martensitic NiTi, e.g,. [33–37]. Thus, it is well known that the degree of cold work represents a critical parameter, which affects twin types as well as the crystallographic character of intervariant twinning planes. With increasing level of cold work, (11-1) type I twins become dominant, and special-twinned microstructures with substructural bands, wavy (001) twin boundaries, and wedge-like (111) type I twinning plates evolve [33–37]. At very high deformation levels, local amorphization was reported [37].

Mechanical TIE properties and the underlying deformation mechanisms have so far received limited attention [23–25, 27, 28, 34, 38–40]. Tadaki and Wayman [34] discussed the mobility of twin boundaries in plastically deformed NiTi martensite. They concluded that pre-existing twin boundaries become immobile in the presence of higher dislocation densities. They suggest that the "unusual elastic behavior" is probably related to the appearance/disappearance of micro twins during loading/unloading, as previously observed by Narita et al. [41] in Cu–Ge alloys. About 20 years after the work of Tadaki and Wayman [34], Zheng et al. [24] and Zhao et al. [25] were able to confirm by in situ transmission electron microscopy that indeed (011) microtwins appear/disappear during mechanical cycling. They suggested that this process represents a key deformation mechanism in NiTi SMAs showing the TIE effect. The mechanical behavior of TIE and PE NiTi shape memory alloys has been compared by Zadno and Duerig [27] who showed that TIE allows to store slightly larger elastic energies than PE. Hoshiya et al. [42] observed a mechanical behavior very similar to TIE after neutron irradiation of NiTi.

At present, only little information is available on the mechanical behavior of TIE SMAs [23–25, 27, 28, 34, 38–40]. In the present work, we investigate the TIE effect in equiatomic NiTi SMAs. An attempt is made to characterize the effects of pre-deformation on stress/strain behavior and on the underlying elementary deformation processes using uniaxial tensile testing and dynamic mechanical analysis (DMA).

Experimental Procedure

Production of TIE Wires

In the present study, equiatomic NiTi wires were produced by vacuum induction melting and subsequent thermomechanical processing involving swaging, wire drawing, and subsequent heat treatments. The alloys were prepared by melting high purity Ni pellets and Ti rods in a vacuum induction furnace of type PVA TEPLA VSG 010 in Argon atmosphere at 500 mbar. We took advantage of the Ti-cladding technique [43] which allows to keep contamination during melting at a minimum. The resulting $Ni_{50}Ti_{50}$ ingots had a weight of 1 kg and a diameter of 40 mm. The cast ingots were homogenized at 1000 °C for 10 h under argon atmosphere followed by water quenching. Chemical analysis (details are given in [14, 15]) indicates that the weight percentage of carbon (<0.04 %) and oxygen (<0.011 %) is below the specification of the ASTM F2063-05 standard [44].

The initial 40 mm diameter of the ingots was reduced to 5.5 mm in several hot swaging steps using a swaging device of type R6-4-120-21S (from HMP GmbH, Pforzheim, Germany) using 800 °C/10 min anneals before each step. After deformation, this specific heat treatment results in full recrystallization of the microstructure and is referred to as recrystallization anneal (RA) throughout this work. The degree of swaging deformation φ was calculated by Eq. 1,

$$\varphi = 2\ln\frac{d_I}{d_F}, \tag{1}$$

where d_I represents the initial diameter and d_F the resulting diameter after deformation. Each swaging step was associated with a degree of deformation close to 0.3.

After swaging, the samples were again subjected to RA before they were subjected to further cold work by wire drawing (wire drawing instrument: HMP ZPR 2000 6 from HMP GmbH, Pforzheim, Germany). Wire drawing was carried out at room temperature in several steps, each with a degree of cold work (Eq. 1) of $\varphi = 0.07$. Intermediate RA treatments were performed between three subsequent wire drawing steps. After the final deformation step, the wires were straightened and again subjected to RA. Our procedure establishes a fully recrystallized microstructure with a medium grain size close to 30 μm [45, 46]. The resulting NiTi wires were used for all subsequent mechanical tests, where the processing stress/strain history was no longer considered and the deformation of the as-processed material was reset to $\varphi = 0$. In order to study the effects of pre-deformation on TIE, further wire drawing was carried out at room temperature, such that the material was again deformed in the martensitic state. Wires with diameters of 1.66, 1.6, 1.54, 1.44, 1.34, and 1.25 mm (corresponding to pre-deformation levels of $\varphi = 0.07$, 0.14, 0.22, 0.35, 0.49, and 0.63) were thus obtained. All further details on thermomechanical treatments are given elsewhere [21, 45–47].

Microstructural and Thermal Characterization

Metallographic samples were prepared for optical microscopy by mechanical polishing and by color etching using a solution of 14 g potassium disulfide in 50 ml Beraha I [43, 45, 46, 48]. Optical microscopy was carried out using a Leica DM 4000 M microscope with polarized light. Cross-sectional metallographic samples were prepared parallel to the load axis during wire drawing and parallel to the center of the wires. Grain size distributions were obtained combining a classical line intersection method with quantitative image analysis (software: Aquinto a4i). At least 500 grains were considered for each material state. The effects of cold work on microstructures were further investigated by X-ray

diffraction (XRD). A diffractometer of type Philips X'Pert, equipped with a copper tube, a hybrid monochromator with a 1/4° aperture providing Cu–$K_{\alpha 1}$ radiation, and a X'Celerator line detector were used. The scanning rate was 0.002842°/s, and the increment between two steps was 0.006°. XRD scans were repeated four times to accumulate higher diffraction intensities. The diffraction data were interpreted using the Le Bail refinement implemented in the software MAUD [49, 50]. For sample preparation, four wire specimens were combined to increase the size of the X-ray target. They were mounted in epoxy resin which contained lead glass powder to suppress unwanted reflections. In a final preparation step, the cross sections were vibropolished using an oxide suspension from Microdiamond GmbH (Kempen, Germany).

Differential scanning calorimetry (DSC) was used to characterize the transformation behavior of the materials at ±150 °C. The DSC parameters were chosen in accordance to the ASTM 2004–2005 standard [51]. Heating/cooling rates of 10 K/min were applied. The maximum and minimum temperatures were kept for 3 min. The measurements were carried out in a protective argon atmosphere. The start and finish temperatures of the forward and reverse transformations, M_S/M_F, and A_S/A_F, respectively, were determined using the tangent method. For further details on DSC testing see [14, 52].

Mechanical Analysis

The mechanical behavior of the different material states was investigated using quasi-static and dynamic mechanical analysis. The quasi-static behavior was characterized using a Zwick/Roell test instrument of type Z100. The wire samples had a length of 60 mm. 15 mm on each side were used for gripping. The accessible length for mounting an extensometer was 30 mm. The strain measurement was carried out using an extensometer of type 188553-MultiXtens with 15 mm gage length. Loads were determined using a 100 kN Zwick/Roell type XforceK load cell. A climate chamber of type SFL EC1835 was used to keep the temperature constant at 20 °C. Each experiment started at a pre-stress of 30 MPa with a constant crosshead displacement rate of 0.5 mm/min. Further details on mechanical testing are documented elsewhere [53, 54].

Figure 2 shows a schematic loading/unloading curve of a TIE wire together with the parameters which were retrieved from the mechanical experiments. These include the residual strain ε_{res}, the apparent Young's modulus E, the hysteresis width $\Delta\varepsilon$, and the maximum and minimum stresses σ_{max}/σ_{min}. The parameters E and $\Delta\varepsilon$ were determined at $(\sigma_{max}-\sigma_{min})/2$ as indicated in Fig. 2. It has been pointed out that the apparent Young's modulus accounts
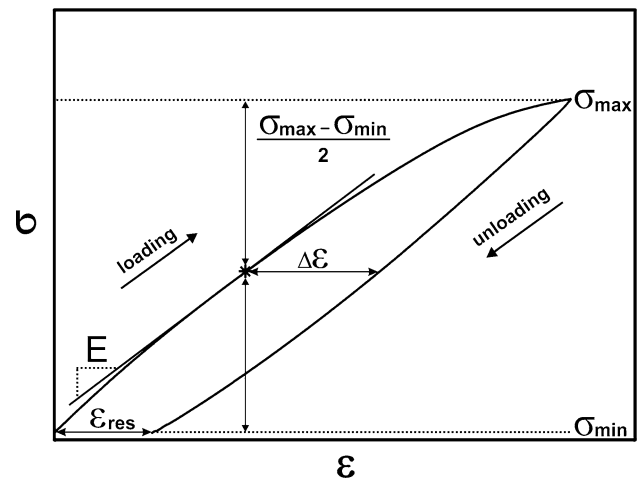
Fig. 2 Schematic illustration showing mechanical key parameters in TIE materials: maximum tensile strength—σ_{max}, apparent Young's modulus—E, residual strain—ε_{res}, and hysteresis width—$\Delta\varepsilon$

for both, elastic as well as small scale twinning-related deformation processes [23, 47].

Dynamic mechanical analysis (DMA) was used to analyze the visco-elastic deformation behavior of TIE wires. In general, DMA allows the characterization of linear-elastic, visco-elastic, and/or visco-plastic material behaviors [55]. In the uniaxial tensile DMA experiments performed in the present study, the sample is subjected to a combination of a static pre-strain ε_{stat} and a superimposed time-dependent dynamic strain amplitude ε_{dyn}. An imposed strain-signal $\varepsilon(t)$ results in a delayed stress response $\sigma(t)$. The delay corresponds to a phase shift δ. From the experiments one can evaluate (1) a storage modulus E' (captures linear-elastic properties) and (2) a loss modulus E'' (accounts for time-dependent effects). The factor tan δ represents a parameter which accounts for the damping capacity of a system [55]. In the present study, a DMA instrument of type 500 N EPLEXOR from Gabo Qualimeter GmbH, Germany was used. A cyclic sinusoidal strain was imposed on NiTi wires of 30 mm gage length (total length = 50 mm), and the corresponding stress response signal was recorded. Specimens were loaded by a static strain ε_{stat} of 0.5 % and superimposed dynamic strain amplitudes ε_{dyn} of 0.02 and 0.25 % (frequency: 10 Hz). The tests started at 150 °C. Testing was performed, while temperatures decreased to −150 °C and subsequent increased back to 150 °C in 2 °C/ min. In 5 K intervals, the storage modulus E', loss modulus E'', and damping factor tan δ were determined. The test parameters were chosen following the DMA standard as outlined in EN ISO 6721-1 [56] and as recommended in previous literature on DMA assessments of SMAs [57–61].

## Results

Microstructural and Thermal Analysis

Figure 3 shows the effect of pre-deformation on the microstructures of stoichiometric NiTi wires. The microstructure of the fully annealed NiTi wire ($\varphi = 0$, starting material for preparation of TIE states) is shown in Fig. 3a. The color etchant reveals both former austenite grains (strong contrast) and martensite twins (small needle-like structures with lower contrast). Grain sizes were measured considering distinguishable prior austenite grain boundaries. Figure 3b and c show the microstructures after medium and high levels of pre-deformation ($\varphi = 0.35$ and 0.63). As the degree of cold work increases, the initially equiaxed grains elongate along the wire drawing direction (indicated by white arrows). To quantify the evolution of microstructure, linear intercept grain sizes were measured parallel and perpendicular to the wire drawing direction and are presented in the cumulative probability nets in Fig. 3d and e. These represent numerically linearized

Gauss distributions. The horizontal gray line at 50 % shows the median value of the grain size. In the wire drawing direction, the average grain size for $\varphi = 0$ is 14 μm. Grain sizes increase to 18 and then to 22 μm as the degree of cold work increases to 0.49 and 0.63. Average grain sizes (50 % values in probability nets) normal to the wire drawing direction were determined as 11 μm ($\varphi = 0$), 7 μm ($\varphi = 0.49$), and 6 μm ($\varphi = 0.63$).

Figure 4 shows how XRD peak profiles are affected by processing. It presents diffractograms for the wires with $\varphi = 0$, 0.07, 0.35, and 0.63. Diffracted intensities are presented in a 2θ angular range from 37 to 47°. The diffracted intensities were interpreted taking the crystal structures of B19′ (martensite) [62, 63], B2 (austenite) [64], R phase (a second martensitic phase in the NiTi system) [65], and TiC (carbide) [66] into account. It was not possible to clearly rationalize each single diffraction peak, due to the fact that XRD experiments were performed on slightly oxidized wires where additional surface phases contribute to the diffracted intensities. The undeformed wire mainly consist of B19′, only small volume fractions of
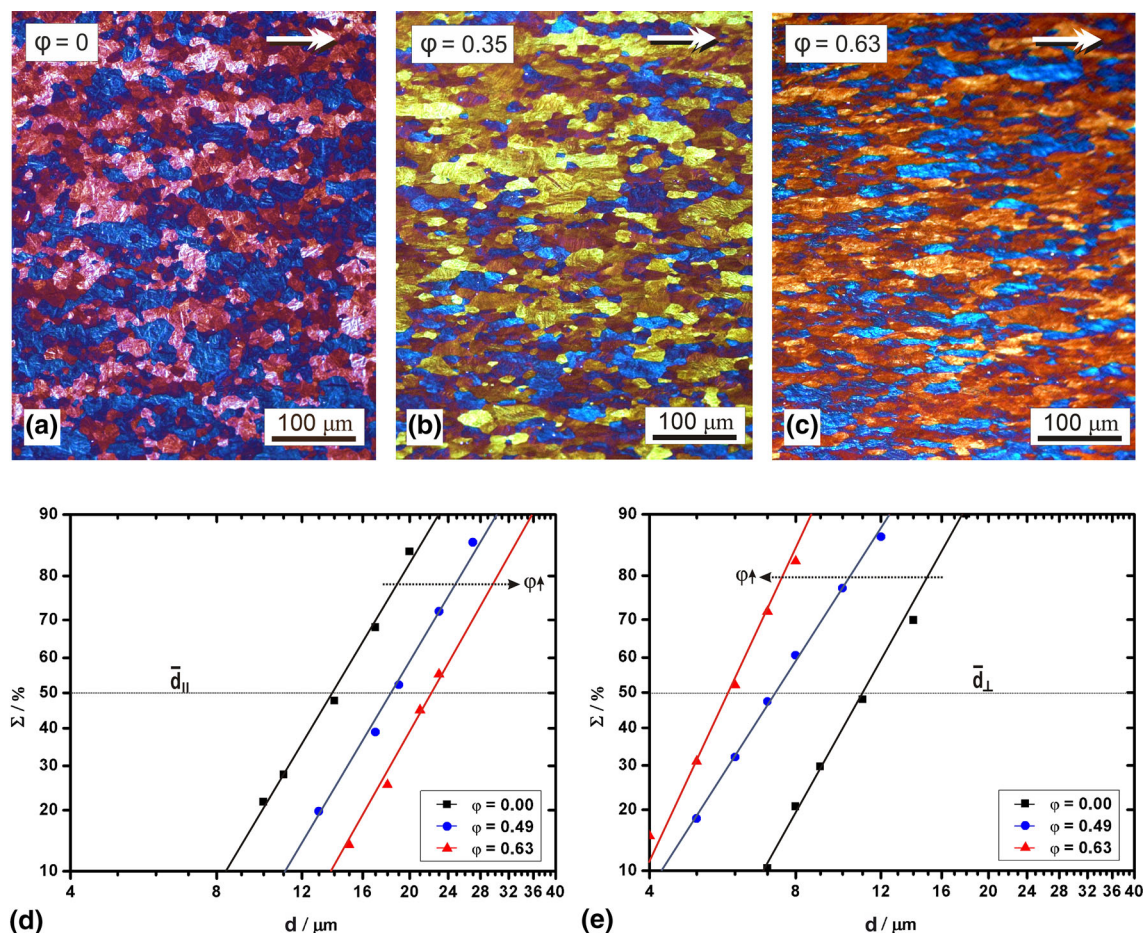
Fig. 3 Effect of cold work on microstructures. a–c Optical micrographs of NiTi wires with different degrees of cold work φ. a $\varphi = 0$. b $\varphi = 0.35$. c $\varphi = 0.63$. d, e Grain size distributions determined, d parallel and e perpendicular to the wire drawing direction
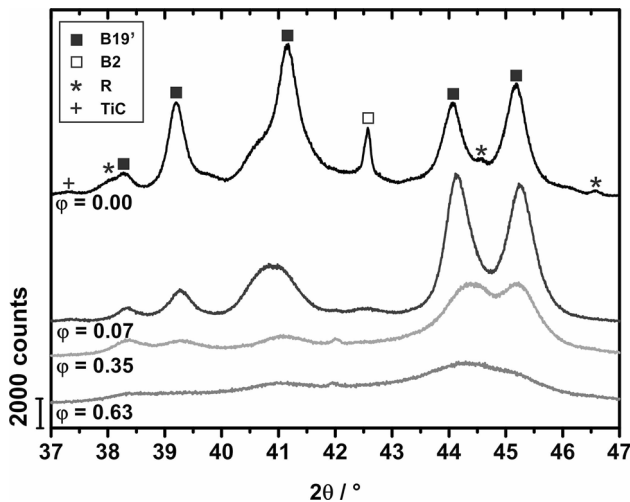
**Fig. 4** XRD scans for NiTi wires with different levels of cold work

B2, R phase, and TiC (common impurity in VIM-melted NiTi [67]) are present. After wire drawing, the peak intensities change and peak widths slightly increase. After mild pre-deformation ($\varphi = 0.07$), the austenite peak disappears. In the case of the strongly deformed wire ($\varphi = 0.63$), no clear diffraction peaks can be distinguished. This suggests that strong cold work leads to partially amorphous material states.

Figure 5 shows the effect of cold work on phase transformations in $Ni_{50}Ti_{50}$ wires. Figure 5a shows DSC charts, while Fig. 5b shows heat affects associated with the DSC peaks. In the fully annealed condition ($\varphi = 0$), the austenite/martensite transition results in a pronounced endothermic peak with $M_S = 61.2$ °C and $M_F = 17.9$ °C, Fig. 5a. These values are in line with what one would expect for the alloy composition considered in the present study [14, 15]. The reverse transformation during heating

results in a pronounced endothermic peak characterized by $A_S = 62.6$ °C and $A_F = 103.5$ °C. As the degree of wire thickness reduction increases, the DSC charts flatten out and the areas associated with DSC peaks (corresponding to latent heats of transformation) decrease. For materials with $\varphi > 0.35$, no transformation peak can be detected on heating and cooling. Figure 5b shows the evolution of the latent heats ΔH with increasing degrees of cold work φ. Note that the absolute values of the enthalpies associated with the endothermic and exothermic heat effects are identical. As φ reaches 0.35, latent heats can no longer be detected. In line with previous findings [46], the dislocations which were introduced by this degree of cold work impede the reverse transformation on heating.

Quasi-static Mechanical Behavior

Figure 6 shows loading/unloading stress/strain curves from the initial material ($\varphi = 0$) and a mildly deformed ($\varphi = 0.07$) state. Both experiments were performed in strain control and maximum strains ε_{max} of 4 % were imposed. Both experiments shown in Fig. 6 consisted of 10 loading/unloading cycles. In case of the undeformed wire, initial straining results in increasing stresses until a stress/strain plateau starts at a strain close to 1 %. This is related to a pseudoplastic deformation of martensite [1–5]. After the first unloading, about 0.4 % strain is recovered, and a high residual strain (ε_{res}) remains, which is due to pseudoplasticity [1–5]. Further mechanical cycling is associated with no significant further evolution of residual strains. Figure 6 shows that already a mild level of pre-deformation drastically alters the mechanical behavior of our material. A pre-strain of $\varphi = 0.07$ fully suppresses the pseudoplastic stress/strain plateaus of the starting material. The maximum stress reached at the end of the loading
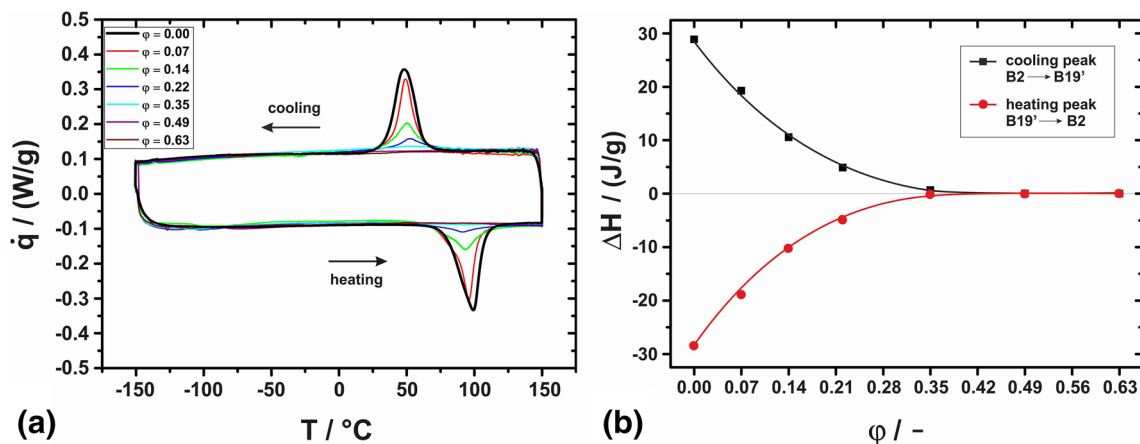

Fig. 5 Effect of cold work on phase transformation behavior. **a** DSC charts of NiTi wires with different cold work levels. **b** Latent heats of forward (B2 → B19′) and reverse transformations (B19′ → B2) as obtained from transformation peaks in DSC charts
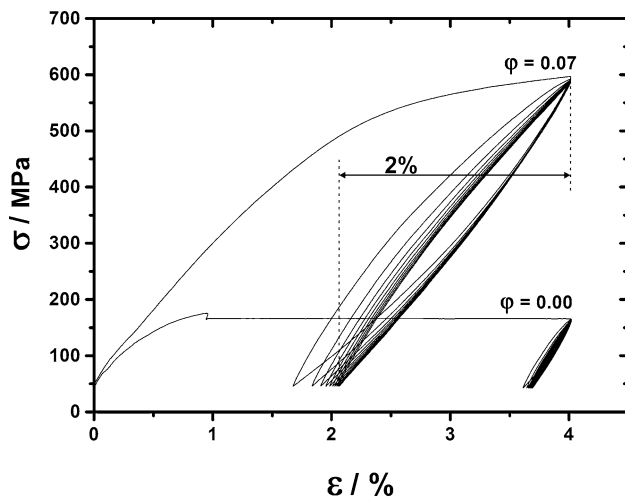
Fig. 6 Comparison of the tensile behavior of the fully annealed starting material ($\varphi = 0$) and a slightly cold drawn ($\varphi = 0.07$) NiTi wire, both subjected to 10 loading and unloading cycles with a maximum imposed strain of $\varepsilon_{max} = 4$ %

cycle increases by a factor of 4. This mechanical behavior is in line with what was reported on TIE materials in the literature [23, 24, 27, 28, 38, 40]. It underlines that a small amount of pre-deformation is sufficient to establish TIE in NiTi. A cyclic reversible strain of 2 % (double arrow in Fig. 6) can be achieved for a strain amplitude of $\varepsilon_{max} = 4$ %. However, the first loading/unloading cycle causes a permanent residual strain of the same order of magnitude. During further cycling, the residual strain slightly increases. The cycle by cycle increase becomes smaller with increasing cycle numbers, in line with what has been reported in the literature for PE NiTi [9].

The cyclic loading/unloading behavior was evaluated for all TIE states. Experiments were performed imposing maximum strains of 2, 3, and 4 %. Figure 7 exemplarily shows the cyclic mechanical behavior of wires which were subjected to cold work levels of $\varphi = 0.07$ (Fig. 7a), 0.35 (Fig. 7b), and 0.63 (Fig. 7c). For each material, 10 loading and unloading cycles were conducted with different maximum strains. Figure 9a–c shows cigar-shaped loading/unloading stress/strain hysteresis curves with a small hysteresis area. The results suggest that the mechanical behavior of the wires is strongly affected by processing parameters. The level of cold work φ and the test conditions (maximum imposed strain ε_{max} and number of cycles) affect the cyclic behavior. With increasing level of pre-deformation, the slopes of the loading/unloading curves become steeper, less residual strain is accumulated during mechanical cycling, and the width of the mechanical hysteresis decreases. The corresponding changes in apparent modulus of elasticity (E), maximum stress (σ_{max}), residual strain (ε_{res}), and hysteresis width ($\Delta\varepsilon$) were evaluated for
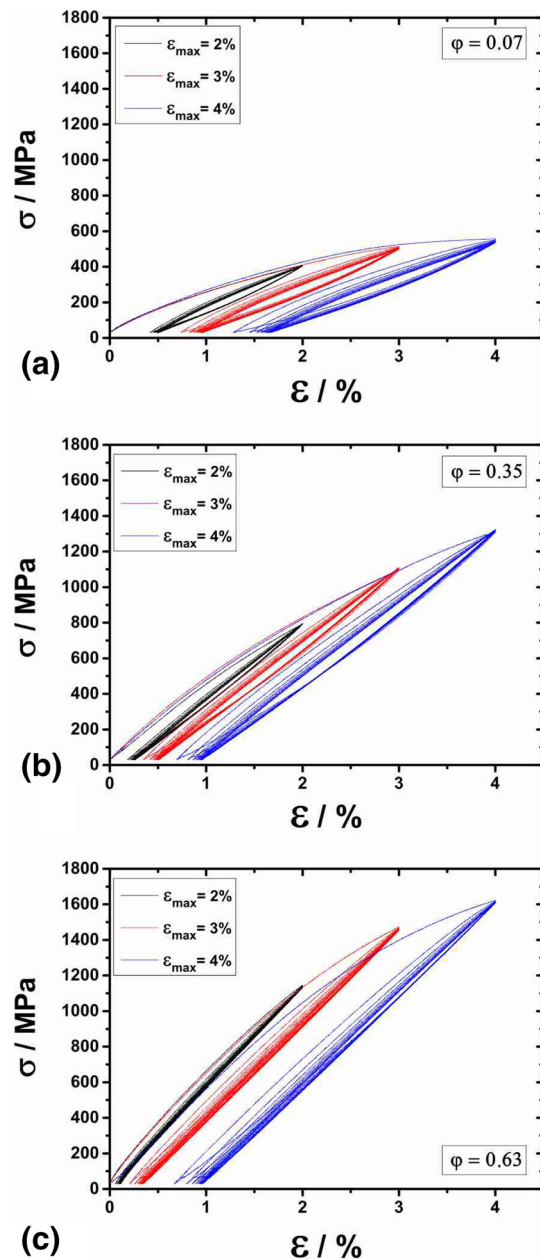
Fig. 7 Quasi-static tensile behavior of NiTi wires with different degrees of cold work, **a** $\varphi = 0.07$, **b** $\varphi = 0.35$, and **c** $\varphi = 0.63$. Ten loading and unloading cycles with maximum imposed strains of $\varepsilon_{max} = 2$, 3, and 4 % were conducted
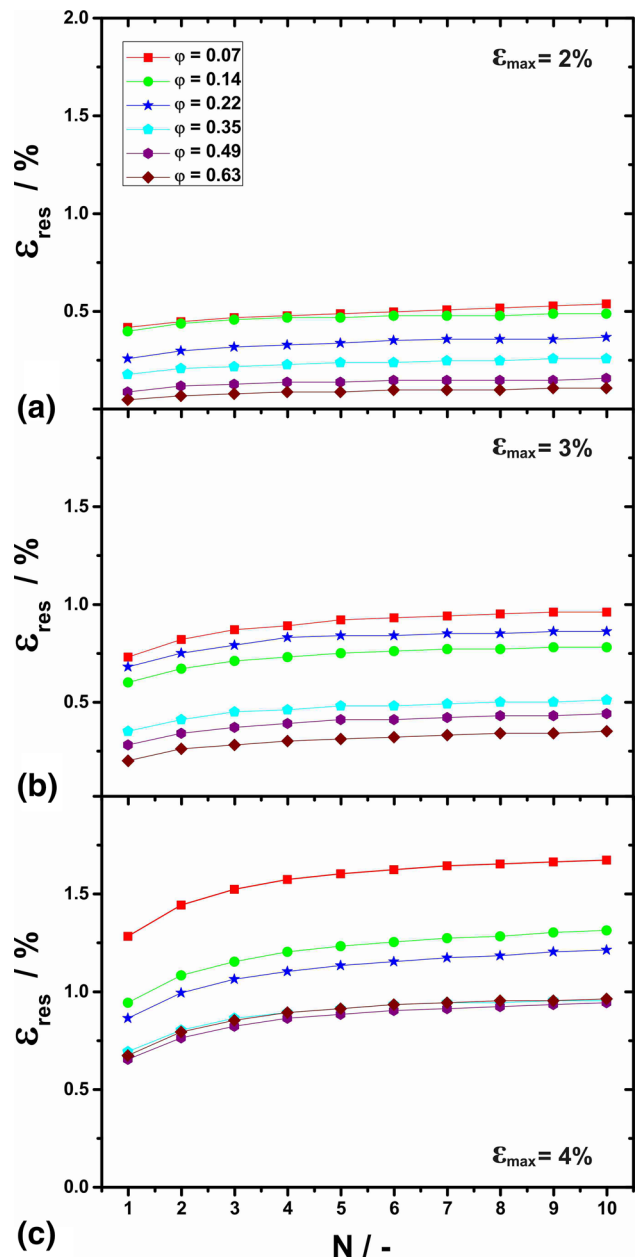
all material states and testing conditions. The results are presented in Figs. 8, 9, and 10.

Figure 8 shows the dependence of the apparent Young's modulus (Fig. 8a) and maximum stresses (Fig. 8b) on processing conditions. Figure 8a documents how an increase in the level of cold work affects the apparent Young's modulus for two different material states. The first dataset ($N = 1$) represents the mechanical behavior in the first loading/unloading cycle, whereas $N = 10$ reveals the
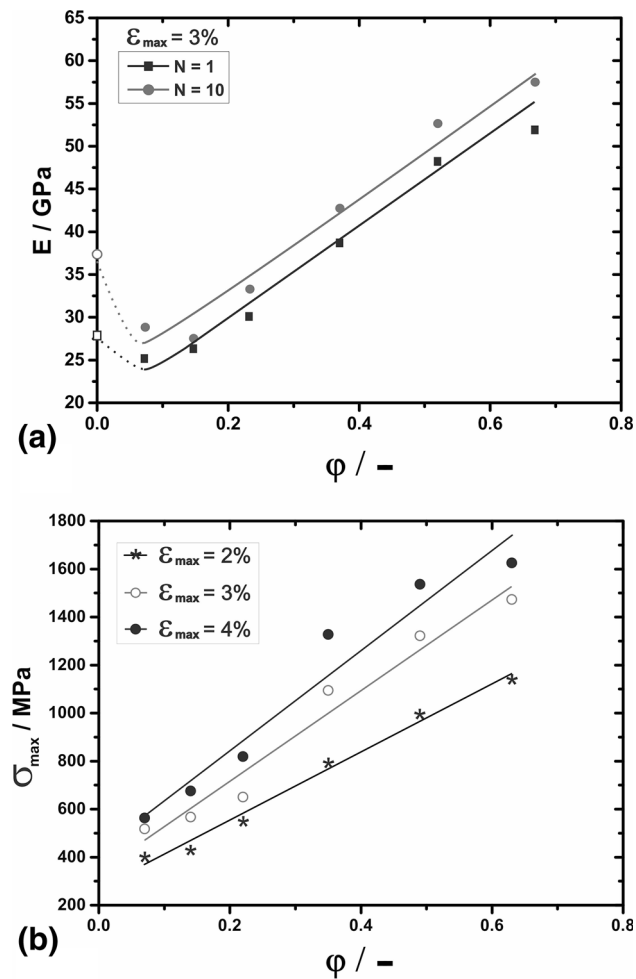
Fig. 8 Effect of the degree of cold work on **a** the apparent Young's modulus and **b** the highest stress obtained from tensile tests with maximum imposed strains of ε_{max} = 2, 3, and 4 %. The *white-filled symbols* in **a** represent data from the pseudoplastic wire, which does not show the TIE effect

Fig. 9 Cyclic stability of mechanical behavior in TIE NiTi. Influence of the number of cycles N on the residual strain ε_{res} for different cold work levels and different maximum imposed strains of **a** 2 %, **b** 3 %, and **c** 4 %

sample stiffness in the 10th cycle. Mechanical cycling results in a slight increase of the apparent Young's modulus. The slope of the resulting Young's modulus versus pre-deformation φ curves is not affected by cycling. In the first cycle, the mildly deformed wire ($\varphi = 0.07$) exhibits a stiffness of only 30 GPa. This value increases with an increasing level of cold work, such that a value of 57 GPa is obtained for $\varphi = 0.63$. Mechanical cycling results in a decrease of the modulus by about 3–5 GPa. Figure 8a also contains data points from the fully recrystallized starting material ($\varphi = 0$; empty symbols). This material state shows a pseudoplastic behavior (see Fig. 6) and therefore its apparent elastic modulus does not follow the same trend as the TIE wires. The increase of the material stiffness is associated with an increase in maximum stresses (σ_{max}). We note, that wires with high cold work levels reach remarkably high stresses during mechanical cycling. For

example, the wire with the highest level of cold work ($\varphi = 0.63$) reaches about 1600 MPa at an imposed strain of 4 %.

Figure 9 shows how the degree of pre-deformation, different maximum imposed strains, and mechanical cycling affect residual strains which remain after unloading. The results shown in Fig. 9 suggest that for TIE wires an increasing number of cycles results in an increase of residual strains. This increase is most pronounced in the
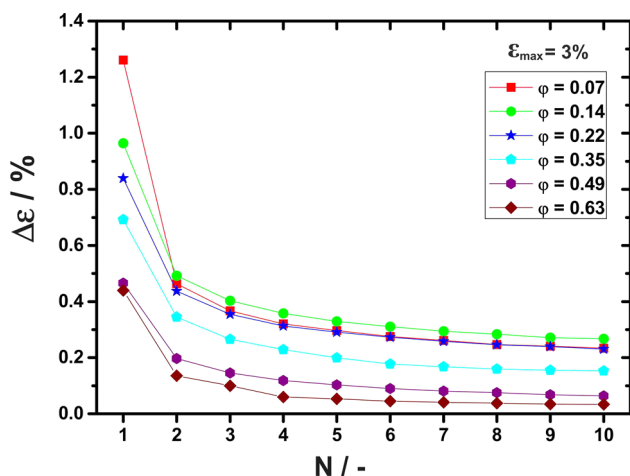
Fig. 10 Cyclic stability of the mechanical behavior in TIE NiTi. Evolution of hysteresis width $\Delta\varepsilon$ during 10 loading/unloading cycles with a maximum imposed strain of $\varepsilon_{max} = 3$ %

first cycle, and it decays during further cycling. The residual strain and its evolution during mechanical cycling strongly depend on the level of cold work and the imposed maximum strain. In general, a more stable mechanical behavior is observed for higher degrees of deformation (brown curves in Fig. 9a–c) and lower imposed strains. For example, the mildly deformed wire ($\varphi = 0.07$) accumulates 0.6 % residual strain within 10 loading/unloading cycles with a strain amplitude of $\varepsilon_{max} = 2$ %, Fig. 9a. An increase in the level of cold work to $\varphi = 0.67$ reduces the accumulated ε_{res} value down to 0.1 %. In contrast, an increase of the loading amplitude ε_{max} to 4 % strain (Fig. 9c) yields a higher residual strain of 1.7 % after 10 cycles for the same material ($\varphi = 0.07$).

Figure 10 presents the effect of mechanical cycling on the evolution of hysteresis width $\Delta\varepsilon$ for wires with different cold work levels. The maximum imposed strain was 3 %. In general, wires with low degrees of deformation exhibit a larger mechanical hysteresis width (e.g., close to 1.26 % for the $\varphi = 0.07$ wire). The hysteresis width significantly decreases with increasing plastic deformation, as well as during mechanical cycling. This decrease is most pronounced after the first cycle in samples with low cold work levels. In the case of the mildly deformed wire ($\varphi = 0.07$), the hysteresis width decreases from $\Delta\varepsilon = 1.26$ to 0.22 % within 10 cycles. In contrast, under the same test conditions, $\Delta\varepsilon$ decreases from 0.45 to 0.02 % for the strongly deformed wire ($\varphi = 0.63$).

Dynamic Mechanical Analysis

In the present work, we use DMA to characterize the effect of pre-deformation on the time-dependent stress response of the TIE twin structure to strain-controlled cyclic loading.

Figure 11 shows the plots of the storage modulus (E') and damping factor tan δ versus temperature T for fully recrystallized ($\varphi = 0$) NiTi wires, subjected to a static strain of $\varepsilon_{stat} = 0.5$ %. Two different strain amplitudes ($\varepsilon_{dyn} = 0.25$ and 0.02 %, respectively) were chosen for the experiments subjected to ±150 °C heating/cooling cycles. In Fig. 11, the upper case letters C and H characterize the cooling and heating parts of a full cycle. The vertical dashed lines shown in Fig. 11 represent martensite start (M_S) and finish (M_F) temperatures which were derived from the DSC chart of the same material state shown in Fig. 5a. We first consider the experiment with a high dynamic strain amplitude of 0.25 %, corresponding to the gray lines seen in Fig. 11. The storage modulus initially slightly decreases from ~70 GPa at 150 °C to ~65 GPa at 70 °C. This decrease is caused by a softening of the austenite lattice when approaching M_S [68]. Between M_S and M_F, the martensitic transformation results in a significant drop of E', followed by a moderate and almost linear increase during further cooling. Heating from -150 °C to 100 °C again results in a moderate decrease of E', until the reverse transformation from martensite to
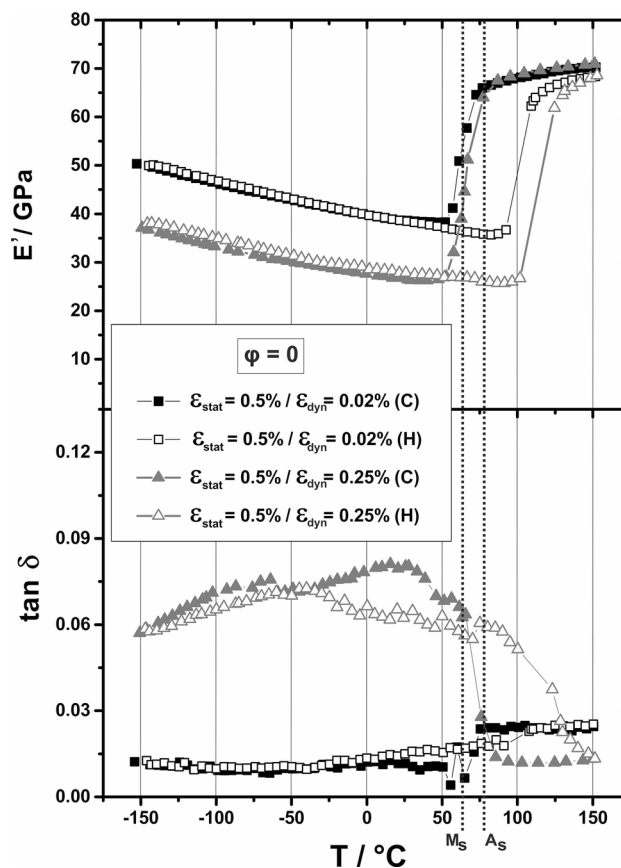
Fig. 11 Plot of storage modulus E' and damping factor tan δ versus temperature T for the fully recrystallized NiTi wires ($\varphi = 0$), which were subjected to a static strain of $\varepsilon_{stat} = 0.5$ % and dynamic strain amplitude of $\varepsilon_{dyn} = 0.26/0.02$ % under heating cooling cycles

austenite produces an abrupt increase between 100 and 130 °C. Both heating and cooling curves limit a hysteresis area, which can be qualitatively compared to the DSC results presented in Fig. 5a. Similar DMA results have been reported in literature for NiTi SMAs [57–61]. The phase transformation processes, which occur during cooling and heating, also manifest themselves through changes in the damping behavior. The tan δ curves in the lower part of Fig. 11 (gray lines) show that the transformation from austenite to martensite is associated with a significant increase in tan δ. This increase of damping capacity is related to time-dependent twin boundary motion as suggested in literature [57–61]. On heating from −150 °C, tan δ decreases at temperatures close to 110 °C due to the reverse transformation.

Both E' and tan δ datasets obtained for the high dynamic strain amplitude of 0.25 % capture the transformation behavior which relies on changes in the martensite twin structure. However, the situation changes when we reduce the dynamic strain amplitude from 0.25 % to only 0.02 %. In this case (black lines), significantly higher E' values are obtained at lower temperatures. Furthermore, no more increase in tan δ is observed after the material has transformed to martensite. This finding suggests that an imposed dynamic strain of 0.02 % is too low to provide significant changes in the twinned martensite microstructure. Therefore, all further DMA experiments were conducted with a dynamic strain amplitude of 0.25 %.

Figure 12 shows changes in the dynamic mechanical properties (storage modulus E' and damping factor tan δ) for NiTi wires subjected to different degrees of pre-deformation. The black reference line represents the behavior of the undeformed $\varphi = 0$ wire. All other material states were subjected to different degrees of cold work. The E' curves in Fig. 12 show that increasing cold work levels reduce the changes in E' and tan δ related to phase transformations on cooling and heating. Furthermore, increasing levels of cold work yield higher E' values at lower temperatures. For example, the undeformed wire exhibits a storage modulus of 37 GPa at −150 °C. An increase in pre-strain level to $\varphi = 0.67$ provides a higher E' values of 59 GPa. All E' curves of strongly deformed wires show an almost linear behavior during cooling and heating. Cold work reduces the damping tan δ. This finding suggests that strongly deformed microstructures impede twinning processes during cyclic straining of TIE NiTi.
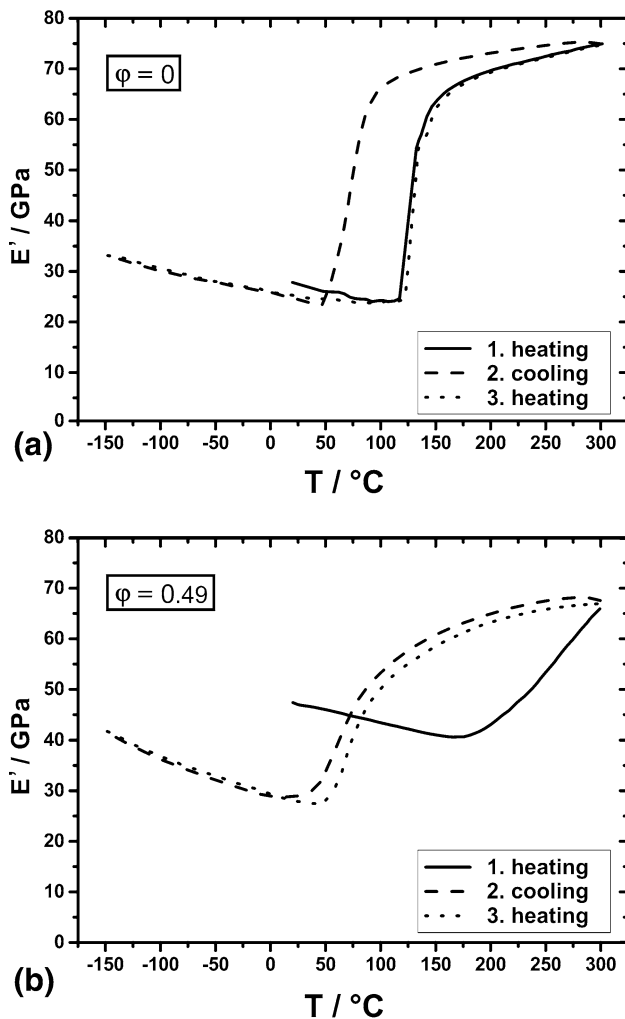
Thermal Stability of the TIE Effect

In order to asses thermal stability of the TIE effect, undeformed and cold drawn wires were subjected to strain-controlled loading in the DMA at temperatures between 300 and −150 °C. This temperature range is larger than that which was
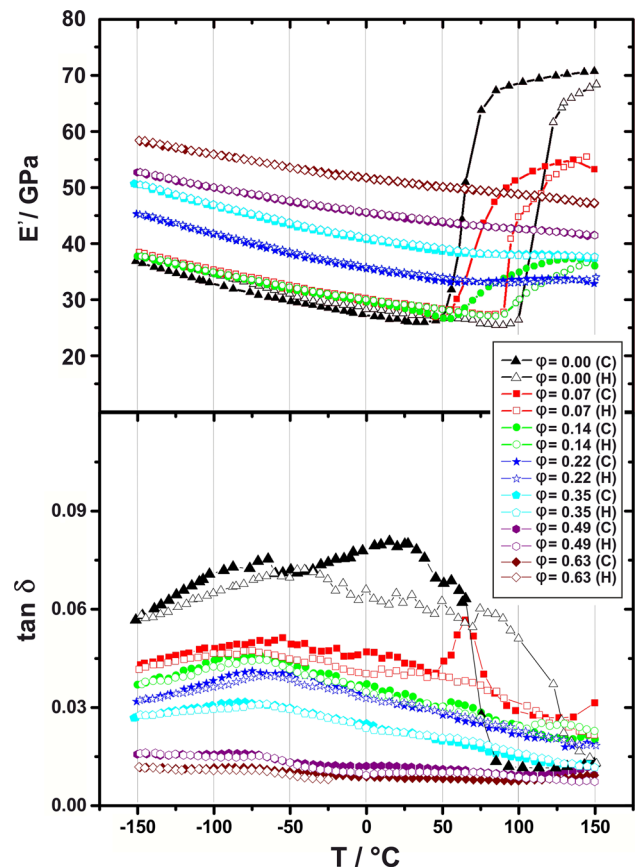
Fig. 12 Effect of cold work φ on dynamic mechanical behavior during cooling (C) and heating (H). $\varepsilon_{stat} = 0.5$, $\varepsilon_{dyn} = 0.25$ %

considered in previous experiments (Figs. 12, 13). The wires were first heated up to 300 °C, then cooled down to −150 °C, and subsequently again heated up to 300 °C. Figure 12a shows the evolution of the storage modules during thermo-mechanical cycling for the undeformed wire which shows qualitatively the same behavior as discussed in the previous section. First, during heating, the transformation from martensite to austenite results in an abrupt increase of E'. Then, second, the martensitic transformation results in a sudden drop of the storage modulus. The second heating cycle shows a very similar behavior as observed in the first cycle. This situation differs for plastically deformed wires subjected to the same procedure, shown in Fig. 12b. Figure 12b shows that the material with $\varphi = 0.49$ shows a higher storage modulus in the early stages of the first heating step, where no indications for phase transformation processes were observed. This is in line with results presented in Fig. 13. However, when reaching ∼160 °C, the evolution of E' deviates from a straight line, and further heating results in a significant increase of the storage modulus. In the subsequent cooling step, the material shows a clear drop of E' which can be interpreted as an evidence for a martensitic transformation. We note, that the same material does not show this type of

Fig. 13 Evaluation of the thermal stability of the TIE effect. Plots of the storage modulus E' versus temperature T for **a** undeformed NiTi wires ($\varphi = 0$) and **b** cold worked NiTi wires ($\varphi = 0.49$), at a static strain of $\varepsilon_{\text{stat}} = 0.5 \%$ and dynamic strain amplitude of $\varepsilon_{\text{dyn}} = 0.25 \%$. The wires were (1) heated to 300 °C, (2) cooled to −150 °C, and (3) again heated to 300 °C

behavior after heating to only 150 °C, as shown in Fig. 13. During the third experimental step, the wire again shows a transformation-related change in E', which indicates a transformation from martensite to austenite. The experimental data presented in Fig. 13b suggest that recovery processes at temperatures exceeding ∼160 °C result in microstructures with low dislocation densities, where martensitic phase transformations are no longer suppressed.

Discussion

Microstructures and Thermal Stability

The present work shows that the degree of pre-deformation represents a key parameter for the production of TIE

SMAs. It strongly affects microstructures and governs mechanical behavior. It has been extensively discussed in the literature how martensitic twin structures evolve with increasing amounts of cold work, e.g., [33–37]. The present work shows that cold work moreover affects prior austenite grain sizes and grain morphologies, Fig. 3. The XRD results in Fig. 4 reveal additional microstructural aspects. Thus Fig. 4 shows that a small volume fraction of austenite was present in the initial material used to produce TIE wires. The presence of austenite is related to the relatively low M_F temperature of the wire (see $\varphi = 0$ wire in DSC chart in Fig. 5a). The fact, that even small amounts of pre-deformation fully eliminate austenite (see diffractograms for $\varphi = 0$ and $\varphi = 0.07$ in Fig. 4) indicates that stress-induced martensite forms during wire drawing, which is later on plastically deformed. Furthermore, a small volume fraction of R phase was detected in the undeformed sample. The occurrence of R phase was not expected since this phase is known to occur only after alloying, aging, or grain size refinement (e.g., [5, 29, 52]). However, the presence of R phase is less important for the scope of the present work. Further efforts are required to confirm and to rationalize the presence of R phase in our material, and to fully exclude effects of sample preparation artifacts. Applying higher degrees of pre-deformation result in higher dislocation densities, as can be seen from the XRD peak broadening in Fig. 4. The corresponding dislocations impede phase transformation processes. This explains the decrease in latent heats as observed in our DSC experiments, Fig. 5b. The XRD data presented in Fig. 4 also indicate that amorphization occurs during wire drawing, which is in line with findings reported in literature [37, 69, 70]. However, in the case of the strongly deformed ($\varphi = 0.63$) wire, no clear diffraction peaks were obtained. This finding suggests that the sample is at least partially amorphous. It was reported by Ewert et al. [69] that after a plastic deformation of the order of 0.7 (true strain), between 5 and 10 % of the volume of NiTi are amorphous. The results of the present study suggest that this even holds for higher volume fraction in our material. However, at present we cannot provide precise quantitative data on amorphous volume fractions on the basis of our θ–2θ XRD scans, since the deformed material is strongly textured. Further work is required to verify this finding.

In the present work, an attempt was made to characterize the thermal stability of plastically deformed microstructures in NiTi. The data from our DMA experiment in Fig. 13 show an increase of the storage modulus during heating up to 160 °C. We assume that this increase in E' is related to a transformation from plastically deformed martensite to austenite. In the corresponding temperature regime, the high driving force for the reverse transformation might restore the parent phase. In addition, recovery

processes might occur and facilitate the transformation back to austenite. Recovery processes reduce dislocation densities, and thus re-establish the ability of the material to undergo phase transformation during heating and cooling [71]. The temperature regime close to 160 °C might appear as too low for recovery. However, diffusion-related processes have been reported in literature to occur in similar temperature ranges [72, 73]. The results in Fig. 13 show that 160 °C represents an upper limit for the TIE effect.

Mechanical Behavior of TIE NiTi

A small level of pre-deformation ($\varphi = 0.07$) is sufficient to eliminate the initial pseudoplastic behavior and to establish the TIE effect in stoichiometric NiTi, Figs. 6 and 7a. However, only relatively moderate reversible strains can be obtained (e.g., 2.3 % for maximum imposed strains of 4 %) since mechanical loading is associated with large residual strains, Figs. 7 and 9. Our results show that highest reversible/lowest residual strains can be obtained for high cold work levels (e.g., $\varphi = 0.63$), Figs. 7 and 9. A wire with a cold work level of $\varphi = 0.63$ yields 3.1 % reversible strain on unloading from 4 % maximum strain. It is interesting to note that strongly deformed material states, where one would expect that dislocations and amorphous regions impede twin boundary mobility, nevertheless provide high reversible strains and show a high cyclic stability, Figs. 7 and 9.

The degree of pre-deformation in TIE wires strongly affects different aspects of their mechanical behavior. It not only improves the ability to recover high imposed strains after mechanical loading (Figs. 7 and 9). It moreover affects apparent Young's modulus (Fig. 8a) and mechanical hysteresis width (Fig. 10). The apparent Young's modulus, which captures both elastic and twinning-related deformation processes, increases with the degree of deformation (Fig. 8a). This behavior has also been mentioned in [74], but not studied in detail. We assume that this behavior can be rationalized on the basis of a scenario where wire drawing in the martensitic state not only results in higher dislocation densities but it moreover results in a martensite texture change. This assumption is supported by the XRD data presented in Fig. 4. Figure 4 shows that wire drawing results in strong changes in diffraction peak intensities (compare peak intensity evolution for different diffraction peaks of $\varphi = 0$ and $\varphi = 0.07$ wires). It seems reasonable to assume that these changes in peak intensities are related to changes in martensite texture during processing. Preliminary results on martensite textures documented in [47] also support this assumption (see Figs. 4.22 and 4.24 in [47]). An additional contribution to the increase of the apparent Young's modulus during wire drawing may result from a high density of dislocations, which impede

twinning processes [34], or from amorphization during wire drawing. Further work is required to clarify this point.

We move on to the cyclic mechanical behavior in TIE NiTi. Our results show that cyclic loading and unloading of TIE wires results in an accumulation of residual strain (Fig. 9), an increase in apparent Young's modulus (Fig. 8a), and in a decrease in hysteresis width (Fig. 10). Similar phenomena are known for NiTi SMAs which show pseudoelasticity or a thermal shape memory effect. These effects are documented for PE NiTi in the literature and they are often referred to as functional fatigue (e.g., [9, 73, 75]). In the case of SMAs showing PE or the 1WE, functional fatigue is related to the generation of microstructural defects, such as dislocations and stabilized martensite during repeated phase transformations [21, 30, 73, 75–77]. This is not the case for TIE SMAs, where phase transformations are not involved. We therefore expect that changes in the mechanical behavior are related to the presence of a certain concentration of mobile dislocations. These dislocations may not only account for irreversible plastic deformation. Moreover, they may well stabilize certain preferentially oriented martensite variants, as discussed in [73, 78], which in turn affects geometry evolution during cycling.

Elemental Deformation Mechanisms

The present work suggests that the TIE effect is generally associated with relatively high mechanical stresses during mechanical loading, Fig. 8b. Therefore, the deformation behavior in TIE wires cannot solely rely on twinning-related processes. A certain fraction of the total strain has to be related to conventional elasticity. We note that the 'real' Young's modulus of B19′ martensite in NiTi is sufficiently low [79–81], such that relative large strains can be obtained just by a conventional elastic deformation. Nevertheless, our results provide evidence that loading and unloading of TIE wires are associated with changes in twinned martensite microstructures. The tensile curves in Figs. 6 and 7 show a hysteresis, and, a considerable damping is observed, Figs. 11 and 12. Figure 14 demonstrates that a correlation exists between damping and hysteresis width. In Fig. 14, the damping tan δ is plotted as a function of the hysteresis width $\Delta\varepsilon$ for TIE wires pre-deformed to different levels of cold work. The data points were retrieved from Fig. 10 (maximum imposed strain 3 %) and Fig. 12 for a temperature of 20 °C on heating. Figure 14 shows a striking result: All data points obtained from the different materials fall on one common line through zero. Our findings confirm that there is a clear coupling between tan δ and $\Delta\varepsilon$. Most importantly, Fig. 14 shows that both tan δ and $\Delta\varepsilon$ continuously decrease with an increasing amount of pre-deformation. These findings suggest that TIE wires
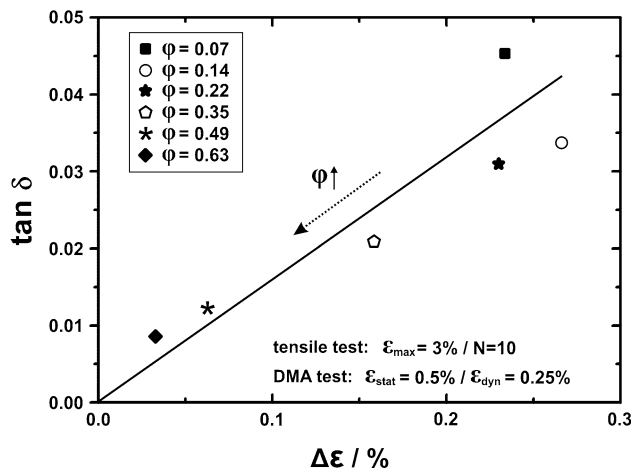
Fig. 14 Correlation between hysteresis width $\Delta\varepsilon$ (10th loading/unloading cycle) and tan δ. The data points were retrieved from Figs. 10 and 12 for a temperature of 20 °C on heating

with low degrees of pre-deformation show the strongest microstructural changes during mechanical loading. In contrast, the microstructures of wires with higher degrees of pre-deformation show a high stability. Our results suggest that the high density of dislocations as well as the presence of amorphous regions (Fig. 4) impede twinning-related processes. Therefore, a larger part of the total deformation has to rely on conventional elasticity in strongly deformed wires. Further work is required to fully rationalize all elementary deformation mechanisms which govern the mechanical behavior of TIE NiTi.

Summary and Conclusions

In the present work, we investigate twinning-induced elasticity (TIE) in NiTi shape memory alloys. From the results obtained in the present study the following conclusions can be drawn:

1. The degree of pre-deformation represents a critical parameter which strongly affects microstructures and mechanical behavior.
2. A relatively low degree of pre-strain is sufficient to establish TIE behavior. Higher degrees of cold work are required to obtain a material state which shows low residual strains and a stable stress strain behavior during mechanical cycling.
3. The microstructural stability restricts exploitation of TIE effect to temperatures below 160 °C.
4. The mechanical behavior in TIE SMAs not only depends on changes which occur in the twinned martensite microstructures. A large part of the overall deformation is based on conventional elasticity. Our findings suggest that higher dislocation densities and the presence of

amorphous regions impede twin boundary mobility. Therefore, the deformation of strongly deformed TIE wires fully relies on conventional elasticity.

References

1. Otsuka K, Waymann CM (1998) Shape memory materials. Cambridge University Press, Cambridge
2. Funakubo H (1987) Shape memory alloys. Gordon and Breach, New York
3. Lagoudas DC (2008) Shape memory alloys: modeling and engineering applications. Springer, New York
4. Otsuka K, Ren X (2005) Physical metallurgy of Ti-Ni-based shape memory alloys. Prog Mater Sci 50(5):511–678
5. Miyazaki S, Otsuka K (1989) Development of shape memory alloys. ISIJ Int 29(5):353–377
6. Valiev R, Gunderov D, Prokofiev E, Pushin V, Zhu Y (2008) Nanostructuring of TiNi alloy by SPD processing for advanced properties. Mater Trans 49(1):97–101
7. Stolyarov VV, Prokof'ev EA, Prokoshkin SD, Dobatkin SB, Trubitsyna IB, Khmelevskaya IY, Pushin VG, Valiev RZ (2005) Structural features, mechanical properties, and the shape-memory effect in TiNi alloys subjected to equal-channel angular pressing. Phys Met Metallogr 100(6):608–618
8. Rahim M, Frenzel J, Frotscher M, Pfetzing-Micklich J, Steegmüller R, Wohlschlögel M, Mughrabi H, Eggeler G (2013) Impurity levels and fatigue lives of pseudoelastic NiTi shape memory alloys. Acta Mater 61(10):3667–3686
9. Eggeler G, Hornbogen E, Yawny A, Heckmann A, Wagner M (2004) Structural and functional fatigue of NiTi shape memory alloys. Mater Sci Eng, A 378(1–2):24–33
10. Robertson SW, Pelton AR, Ritchie RO (2012) Mechanical fatigue and fracture of nitinol. Int Mater Rev 57(1):1–36
11. Robertson SW, Launey M, Shelley O, Ong I, Vien L, Senthilnathan K, Saffari P, Schlegel S, Pelton AR (2015) A statistical approach to understand the role of inclusions on the fatigue resistance of superelastic Nitinol wire and tubing. J Mech Behav Biomed 51:119–131
12. Habijan T, Glogowski T, Kühn S, Pohl M, Wittsiepe J, Greulich C, Eggeler G, Schildhauer TA, Köller M (2011) Can human mesenchymal stem cells survive on a NiTi implant material subjected to cyclic loading? Acta Biomater 7(6):2733–2739
13. Huang HH, Chiu YH, Lee TH, Wu SC, Yang HW, Su KH, Hsu CC (2003) Ion release from NiTi orthodontic wires in artificial saliva with various acidities. Biomater 24(20):3585–3592
14. Frenzel J, Wieczorek A, Opahle I, Maaß B, Drautz R, Eggeler G (2015) On the effect of alloy composition on martensite start temperatures and latent heats in Ni-Ti-based shape memory alloys. Acta Mater 90:213–231
15. Frenzel J, George EP, Dlouhy A, Somsen C, Wagner MFX, Eggeler G (2010) Influence of Ni on martensitic phase transformations in NiTi shape memory alloys. Acta Mater 58(9):3444–3458
16. Sehitoglu H, Jun J, Zhang X, Karaman I, Chumlyakov Y, Maier HJ, Gall K (2001) Shape memory and pseudoelastic behavior of 51.5% Ni-Ti single crystals in solutionized and overaged state. Acta Mater 49(17):3609–3620

17. Discussions at the SMST (2015) Conference. UK, Estone/Chipping Norton, 2015

18. Morgan NB (2004) Medical shape memory alloy applications—the market and its products. Mater Sci Eng, A 378(1–2):16–23

19. Van Humbeeck J (1999) Non-medical applications of shape memory alloys. Mater Sci Eng, A 273–275:134–148

20. Duerig T, Pelton A, Stöckel D (1999) An overview of nitinol medical applications. Mater Sci Eng, A 273–275:149–160

21. Jaeger S, Maaß B, Frenzel J, Schmidt M, Seelecke S, Kastner O, Eggeler G (2015) On the widths of the hysteresis of mechanically and thermally induced martensitic transformations in Ni-Ti based shape memory alloys. Int J Mater Res 106(10):1029–1039

22. Olbricht J, Yawny A, Pelegrina JL, Dlouhy A, Eggeler G (2011) On the stress-induced formation of R-phase in ultra-fine-grained Ni-rich NiTi shape memory alloys. Metall Mater Trans A 42A(9):2556–2574

23. Hornbogen E (1995) On the term pseudo-elasticity. Z Metallkd 86(5):341–344

24. Zheng YF, Huang BM, Zhang JX, Zhao LC (2000) The microstructure and linear superelasticity of cold-drawn TiNi alloy. Mater Sci Eng, A 279(1–2):25–35

25. Zhao LC, Zheng YF, Cai W (2005) Study of deformation micromechanism in cold-deformed TiNi based alloys. Intermetall 13(3–4):281–288

26. Rossin P (2003) US Patent 6,557,993: Eyeglasses and parts thereof made with specially processed NiTi shape memory alloy (2003)

27. Zadno GR, Duerig TW (1989) Linear and non-linear superelasticity in NiTi. MRS Int'l Mtg Adv Mater 9:201–209

28. Andreasen GF, Morrow RE (1978) Laboratory and clinical analyses of nitinol wire. Am J Orthodont 73(2):142–151

29. Waitz T, Antretter T, Fischer FD, Simha NK, Karnthaler HP (2007) Size effects on the martensitic phase transformation of NiTi nanograins. J Mech Phys Solids 55(2):419–444

30. Delville R, Malard B, Pilch J, Sittner P, Schryvers D (2011) Transmission electron microscopy investigation of dislocation slip during superelastic cycling of Ni-Ti wires. Int J Plast 27(2):282–297

31. Frick CP, Ortega AM, Tyber J, Maksound AEM, Maier HJ, Liu YN, Gall K (2005) Thermal processing of polycrystalline NiTi shape memory alloys. Mater Sci Eng, A 405(1–2):34–49

32. Miyazaki S, Ohmi Y, Otsuka K, Suzuki Y (1982) Characteristics of deformation and transformation pseudoelasticity in Ti-Ni alloys. J Phys Colloq 43(C4):255–260

33. Zheng YF, Zhao LC, Ye HQ (2001) HREM studies of twin boundary structure in deformed martensite in the cold-rolled TiNi shape memory alloy. Mater Sci Eng, A 297(1–2):185–196

34. Tadaki T, Wayman CM (1980) Crystal-structure and microstructure of a cold-worked TiNi alloy with unusual elastic behavior. Scripta Metall Mater 14(8):911–914

35. Lin HC, Wu SK, Chou TS, Kao HP (1991) The effects of cold-rolling on the martensitic-transformation of an equiatomic TiNi alloy. Acta Metall Mater 39(9):2069–2080

36. Madangopal K, Banerjee R (1992) The lattice invariant shear in Ni-Ti shape memory alloy martensites. Scr Met Mater 27(11):1627–1632

37. Koike J, Parkin DM, Nastasi M (1990) Crystal-to-amorphous transformation of NiTi induced by cold rolling. J Mater Res 5(7):1414–1418

38. Frotscher M, Menges C, Diehl T, Eggeler G (2007) Einfluss von thermomechanischer Behandlung auf die mikrostruktur von pseudoelastischem NiTi am beispiel von komponenten für Brillengestelle. Prakt Metallogr 44(7):317–333

39. Zider RB, Krumme JF (1988) US Patent 4896955 A: eyeglass frame including shape-memory elements (1988)

40. Mercier O, Török E (1982) Mechanical properties of the cold-worked martensitic NiTi type alloys. J Phys 43((NC-4)):267–272

41. Narita N, Yamamoto A, Umemoto T, Takamura JI (1978) Anelastic effect due to deformation twins in Cu-Ge alloy crystals. J Jpn Inst Met 42(12):1190–1199

42. Hoshiya T (1986) Behavior of neutron irradiated Ti-Ni shape memory alloys. In: International conference on martensitic transformation, The Japan Institute of Metals, 865–890

43. Frenzel J, Zhang Z, Neuking K, Eggeler G (2004) High quality vacuum induction melting of small quantities of NiTi shape memory alloys in graphite crucibles. J Alloy Compd 385(1–2):214–223

44. Standard ASTM F2063-05: Standard specification for wrought nickel-titanium shape memory alloys for medical devices and surgical implants

45. Grossmann C, Frenzel J, Sampath V, Depka T, Oppenkowski A, Somsen C, Neuking K, Theisen W, Eggeler G (2008) Processing and property assessment of NiTi and NiTiCu shape memory actuator springs. Mater Werkst Technol 39(8):499–510

46. Frenzel J, Pfetzing J, Neuking K, Eggeler G (2008) On the influence of thermomechanical treatments on the microstructure and phase transformation behavior of Ni-Ti-Fe shape memory alloys. Mater Sci Eng, A 481:635–638

47. Birk T (2015) Untersuchung zur Zwillingselastizität in NiTi(Cu)-Formgedächtnislegierungen. Ruhr-Universität Bochum, Bochum

48. Weck E, Leistner E (1983) Metallographic instructions for color etchants by immersion, Part II: Beraha colour etchants and their different variants. Deutscher Verlag für Schweißtechnik, Düsseldorf

49. Lutterotti L, Bortolotti M, Ischia G, Lonardelli I, Wenk HR (2007) Rietveld texture analysis from diffraction images. Z Kristallogr 26:125–130

50. Lutterotti L, Gualtieri A, Aldrighetti S (1996) Rietveld refinement using Debye-Scherrer film techniques. Eur Powder Diffr 228:29–34

51. Starndard ATSM F 2004-05: Standard test method for transformation temperature of nickel-titanium alloys by thermal analysis

52. Khalil-Allafi J, Dlouhy A, Eggeler G (2002) Ni$_4$Ti$_3$-precipitation during aging of NiTi shape memory alloys and its influence on martensitic phase transformations. Acta Mater 50(17):4255–4274

53. Schäfer A (2010) Werkstoffwissenschaftliche Untersuchungen zur Bildung und Wachstum von Martensit in NiTi-Formgedächtnislegierungen unter Spannung. Ruhr-Universität Bochum, Bochum

54. Schäfer A, Wagner MFX, Pelegrina JL, Olbricht J, Eggeler G (2010) Localization events and microstructural evolution in ultra-fine grained NiTi shape memory alloys during thermo-mechanical loading. Adv Eng Mater 12(6):453–459

55. Ehrenstein GW, Riedel G, Trawiel P (2003) Praxis der thermischen Analyse von Kunststoffen. Carl Hanser Verlag, Munich

56. Standard EN ISO 6721-1: Determination of dynamic mechanical properties (2003)

57. Nespoli A, Passaretti F, Villa E (2013) Phase transition and mechanical damping properties: a DMTA study of NiTiCu shape memory alloys. Intermetall 32:394–400

58. Fan G, Zhou Y, Otsuka K, Ren X, Nakamura K, Ohba T, Suzuki T, Yoshida I, Yin F (2006) Effects of frequency, composition, hydrogen and twin boundary density on the internal friction of Ti$_{50}$Ni$_{50-x}$Cu$_x$ shape memory alloys. Acta Mater 54(19):5221–5229

59. Wu SK, Lin HC (2003) Damping characteristics of TiNi binary and ternary shape memory alloys. J Alloy Compd 355(1–2):72–78

60. Van Humbeeck J (2003) Damping capacity of thermoelastic martensite in shape memory alloys. J Alloy Compd 355(1–2):58–64

61. Sapozhnikov K, Golyandin S, Kustov S, Schaller R, Van Humbeeck J (2006) Anelasticity of B19′ martensitic phase in NiTi and NiTiCu alloys. Mater Sci Eng, A 442(1–2):398–403

62. Kudoh Y, Tokonami M, Miyazaki S, Otsuka K (1985) Crystal-structure of the martensite in Ti-49.2at-percent-Ni alloy analyzed by the single crystal X-ray-diffraction method. Acta Metall Mater 33(11):2049–2056

63. Otsuka K, Sawamura T, Shimizu K (1971) Crystal structure and internal defects of equiatomic TiNi martensite. Phys. Stat. Solidi A 5(2):457–470

64. Wang FE, Buehler WJ, Pickart SJ (1965) Crystal Structure and a unique martensitic transition of TiNi. J Appl Phys 36(10):3232–3239

65. Khalil-Allafi J, Schmahl WW, Toebbens DM (2006) Space group and crystal structure of the R-phase in binary NiTi shape memory alloys. Acta Mater 54(12):3171–3175

66. Aigner K, Lengauer W, Rafaja D, Ettmayer P (1994) Lattice parameters and thermal expansion of Ti($C_x N_{1-x}$), Zr($C_x N_{1-x}$), Hf($C_x N_{1-x}$) and TiN$_{1-x}$ from 298 to 1473 K as investigated by high-temperature X-ray diffraction. J Alloy Compd 215(1–2):121–126

67. Frenzel J, Zhang Z, Somsen C, Neuking K, Eggeler G (2007) Influence of carbon on martensitic phase transformations in NiTi shape memory alloys. Acta Mater 55(4):1331–1341

68. Ren X, Miura N, Zhang J, Otsuka K, Tanaka K, Koiwa M, Suzuki T, Chumlyakov YI (2001) A comparative study of elastic constants of Ti-Ni-based alloys prior to martensitic transformation. Mater Sci Eng, A 312(1–2):196–206

69. Ewert JC, Böhm I, Peter R, Haider F (1997) The role of the martensite transformation for the mechanical amorphisation of NiTi. Acta Mater 45(5):2197–2206

70. Burow J (2010) Herstellung, Eigenschaften und Mikrostruktur von ultrafeinkörnigen NiTi-Formgedächtnislegierungen, Ruhr-Universität Bochum, Bochum

71. Khelfaoui F, Guenin G (2003) Influence of the recovery and recrystallization processes on the martensitic transformation of cold worked equiatomic Ti-Ni alloy. Mater Sci Eng, A 355(1–2):292–298

72. Wagner MFX, Dey SR, Gugel H, Frenzel J, Somsen C, Eggeler G (2010) Effect of low-temperature precipitation on the transformation characteristics of Ni-rich NiTi shape memory alloys during thermal cycling. Intermetall 18(6):1172–1179

73. Grossmann C, Frenzel J, Sampath V, Depka T, Eggeler G (2009) Elementary transformation and deformation processes and the cyclic stability of NiTi and NiTiCu shape memory spring actuators. Metall Mater Trans A 40(11):2530–2544

74. Duerig TW (2006) Some unsolved aspects of Nitinol. Mater Sci Eng, A 438–440:69–74

75. Miyazaki S, Imai T, Igo Y, Otsuka K (1986) Effect of cyclic deformation on the pseudoelasticity characteristics of Ti-Ni alloys. Metall Trans A 17A(1):115–120

76. Atli KC, Franco BE, Karaman I, Gaydosh D, Noebe RD (2013) Influence of crystallographic compatibility on residual strain of TiNi based shape memory alloys during thermo-mechanical cycling. Mater Sci Eng, A 574:9–16

77. Simon T, Kröger A, Somsen C, Dlouhy A, Eggeler G (2010) On the multiplication of dislocations during martensitic transformations in NiTi shape memory alloys. Acta Mater 58(5):1850–1860

78. Kaya I, Tobe H, Karaca HE, Nagasako M, Kainuma R, Chumlyakov Y (2015) Positive and negative two-way shape memory effect in [111]-oriented Ni$_{51}$Ti$_{49}$ single crystals. Mater Sci Eng, A 639:42–53

79. Wagner MFX, Windl W (2008) Lattice stability, elastic constants and macroscopic moduli of NiTi martensites from first principles. Acta Mater 56(20):6232–6245

80. Stebner AP, Brown DW, Brinson LC (2013) Young's modulus evolution and texture-based elastic–inelastic strain partitioning during large uniaxial deformations of monoclinic nickel–titanium. Acta Mater 61(6):1944–1956

81. Wang J, Sehitoglu H (2014) Martensite modulus dilemma in monoclinic NiTi-theory and experiments. Int J Plast 61:17–31